Angewandte Chemie
Eine Zeitschrift der Gesellschaft Deutscher Chemiker

Supporting Information

Detection of Localized Hepatocellular Amino Acid Kinetics by using Mass Spectrometry Imaging of Stable Isotopes

Martijn Arts[+], Zita Soons[+], Shane R. Ellis, Keely A. Pierzchalski, Benjamin Balluff, Gert B. Eijkel, Ludwig J. Dubois, Natasja G. Lieuwes, Stijn M. Agten, Tilman M. Hackeng, Luc J. C. van Loon, Ron M. A. Heeren, and Steven W. M. Olde Damink*

anie_201702669_sm_miscellaneous_information.pdf

Author Contributions

M.A. Conceptualization: Equal; Data curation: Equal; Formal analysis: Lead; Methodology: Equal; Software: Supporting; Writing—original draft: Equal; Writing—review & editing: Equal; Animal experiments: Equal
Z.S. Conceptualization: Equal; Data curation: Equal; Methodology: Equal; Supervision: Lead; Writing—original draft: Equal; Writing—review & editing: Lead
S.E. Conceptualization: Supporting; Methodology: Supporting; Supervision: Supporting; Writing—original draft: Supporting; Writing—review & editing: Supporting
K.P. Supervision: Supporting; Writing—review & editing: Supporting
B.B. Data curation: Supporting; Writing—review & editing: Supporting
G.E. Data curation: Supporting; Software: Lead
L.D. Funding acquisition: Supporting; Methodology: Supporting; Resources: Supporting; Supervision: Supporting; Writing—review & editing: Supporting
N.L. Methodology: Supporting; Animal experiments: Equal
S.A. Writing—review & editing: Supporting; TAHS reagent production: Lead
T.H. Data curation: Supporting; Resources: Supporting; Supervision: Supporting
L.v. Data curation: Supporting; Methodology: Supporting; Resources: Supporting; Writing—review & editing: Supporting
R.H. Conceptualization: Equal; Data curation: Supporting; Funding acquisition: Equal; Methodology: Supporting; Resources: Equal; Supervision: Supporting; Writing—review & editing: Supporting
S.O. Conceptualization: Equal; Funding acquisition: Equal; Methodology: Supporting; Resources: Equal; Supervision: Supporting; Writing—review & editing: Supporting.

Table of Contents

1. Experimental Methods

1.1 Chemicals

L-Phenylalanine (Phe), L-Tyrosine (Tyr), 2,5-Dihydroxybenzoic acid (DHB), trifluoroacetic acid (TFA), disuccinimidyl carbonate (DSC), dimethyl-4-phenylenediamine (DPD), dichloromethane (DCM), and iodomethane were obtained from Sigma-Aldrich (St. Louis, MO, USA), ring-$^{13}C_6$-Phe from Cambridge Isotope Laboratories (Andover, MA, USA). ULC/MS grade acetonitrile (ACN), methanol (MeOH) and deionized water (H_2O) from Biosolve B.V. (Etten-Leur, The Netherlands). P-N,N,N-trimethylamonioanilyl N-hydroxysuccinimidyl carbamate iodide (TAHS) was synthetized according to the protocol previously described with minor modifications.[1] In short, 6.0 g (23.4 mmol) DSC was dissolved in 250 mL of dry ACN to which 3.0 g (22.0 mmol) DPD in 250 mL dry ACN was added dropwise over a period of 45 min. The product was concentrated using rotary evaporation and resuspended in 100 mL ACN and filtered. The filtrate was concentrated and redissolved in 10 mL 4:1 ACN:DCM after which 4 mL iodomethane (8 equiv.) was added and left to react overnight at room temperature. The reaction mixture was filtered to afford 1.91 g of TAHS (6.55 mmol, 29.8% yield over 2 steps). ^{1}H NMR (700 MHz, DMSO-d_6) δ 11.19 (s, 1H) 7.98 (d, *J* = 9.4 Hz, 2H), 7.63 (d, *J* = 9.4 Hz, 2H), 3.59 (s, 9H), 2.84 (s, 4H) ppm. ^{13}C NMR (175 MHz, DMSO-d_6) δ 170.7 (C) 149.3 (C) 142.6 (C) 138.4 (C) 121.7 (CH) 119.3 (CH) 56.5 (CH_3) 25.4 (CH_2). ^{1}H NMR and ^{13}C NMR spectra are shown in Figure S10 and Figure S11. Indium tin oxide (ITO)-coated conductive glass slides were obtained from DELTA Technologies Ltd. (Loveland, CO, USA).

1.2 Animal Experiments

Adult female immune-compromised Crl:NU-Foxn1^{nu} nu/nu nude mice (Charles River, Den Bosch, The Netherlands) were used (*n* = 15). Normal chow diet and water were available ad libitum. Human NCI-H460 non small cell lung carcinoma (NSCLC) cells were suspended in matrigel (BD Biosciences, Breda, The Netherlands) and implanted subcutaneously in the flank of each mouse, as described. [3] Tumor volume was monitored 3 times a week using a Vernier caliper. Once tumors reached a volume of 1000 mm^3, mice were injected with tracer (*n* = 11) or sham solution (normal saline; *n* = 4) to correct for natural Phe enrichments. The mice received a single bolus injection of a 150 mM Phe mixture in normal saline containing 4:6 ring-$^{13}C_6$-Phe:Phe (v:v) as a dose of 1.0 µmol g^{-1} body weight by intravenous administration in the lateral tail vein. Subsequently, the tracer-infused mice were sacrificed at 10 min (*n* = 4), 30 min (*n* = 3), and 60 min (*n* = 4) after injection, and sham-injected mice were sacrificed after 10 min. Tumor and healthy liver were dissected followed by immediate freezing in liquid nitrogen. Blood samples were taken at two time points, prior to tracer infusion from a distal tail vein and from the heart by cardiac puncture upon cervical dislocation. This strategy enables quantification of tracer enrichment at baseline and end-point as a reference for tissue enrichment as described elsewhere.[2] All samples were stored at -80°C. All procedures and experiments were approved by the Animal Ethical Committee of the University of Maastricht.

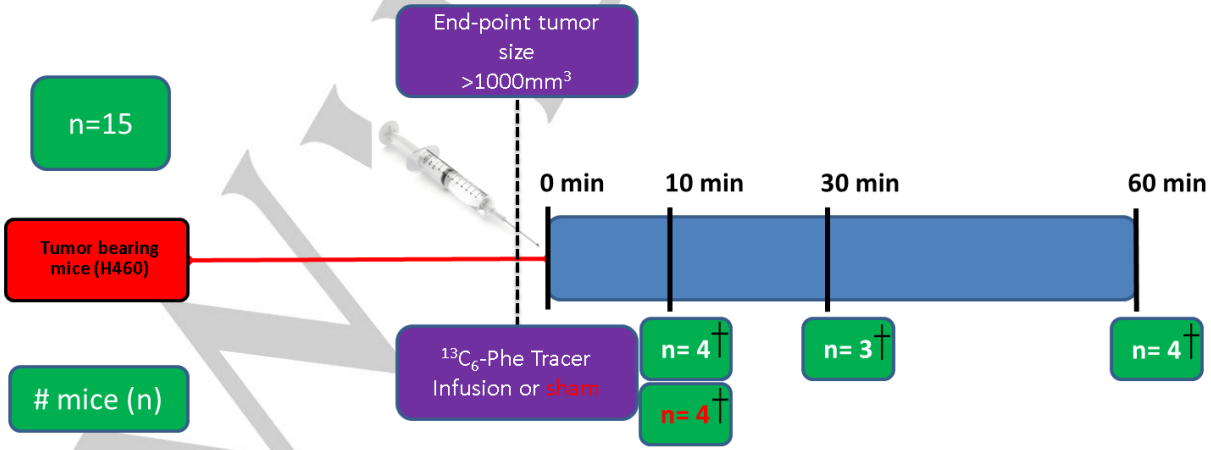

Figure S1. Overview of the animal experiment.

1.3 Tissue Sectioning and Sample Preparation

Serial 10-µm fresh frozen tissue sections were cut at -20°C using a cryostat cryotome (Leica, Rijswijk, The Netherlands). Cryosections were mounted onto ITO-coated glass slides (DELTA Technologies Ltd., Loveland, CO, USA) by thaw-mounting and stored at -80 °C until analysis. Samples were transferred to the desiccator and allowed to dry for 15 min, an important step to obtain optimal spatial information and prevent hydrolysis of the derivatization reagent (data not shown).

A standard solution of 4.4:5 $^{13}C_6$-Phe: Phe (v:v) in H_2O with a final concentration of 500 µM was used to spot 1 µL of standard solution on tissue. Subsequently, the spots were left to dry in the desiccator to fully dry before on-tissue derivatization.

On-tissue derivatization was performed with TAHS, thereby preserving the spatial localization (Figure S12) and enabling MALDI-MS detection. A TAHS solution of 5 mg mL^{-1} in ACN was sprayed onto the sections using the Suncollect sprayer (SunChrom GmbH, Friedrichsdorf, Germany). Three layers of TAHS solution were applied with a flowrate of 10 µL min^{-1} with slight modifications to a protocol described elsewhere.[4] The speed of the spraying in addition to the choice of solvent resulted in preservation of analyte localization and reagent stability. For optimal on-tissue derivatization, samples were incubated at 55 °C for 24 h in a humid environment (50% MeOH in H_2O), necessary to prevent side-reactions of TAHS with the hydroxyl group attached to the phenol group of Tyr.[1] Optimal derivatization was assessed by the highest signal detection reflecting the balance between detection sensitivity and interference of high intensity peaks derived from the matrix or derivatization reagent.

A matrix solution of 30 mg mL^{-1} DHB in 70% MeOH + 0.2% TFA was used. Six layers of fresh matrix were applied with the HTX sprayer (HTX Technologies LLC, Carrboro, NC, USA) with a fixed flowrate of 0.1 mL min^{-1} and a nozzle temperature of 85 °C, followed by immediate MALDI-FTICR-MSI.

The MSI experiments were performed in two technical replicates. The 30 liver sections were distributed onto glass slides in a randomized manner to minimize batch effects and analytical day-to-day variance.

1.4 MALDI-MSI Data Acquisition

High-resolution MALDI-FTICR-MSI experiments were performed with a high-resolution MALDI-FTICR instrument (Solarix, 9.4T, Bruker Daltonics, Bremen, Germany). The MALDI source is equipped with a Smartbeam II ND:YAG UV laser. The measurements were performed with the laser operating at a frequency of 2000 Hz, a laser power of 18%, and 50 shots per pixel. Data were acquired in magnitude mode (positive polarity) in the mass range of 100–1200 *m/z* tuned for the lower masses, using 1 million data points per pixel, and a mass resolution of $1.5e^5$ at 200 *m/z*. Pre-acquisition calibration of the system using a collection of matrix-derived peaks was performed, reaching a maximum mass error of 0.6 ppm. During data acquisition, online lock mass calibration was applied using pre-defined matrix peaks as a reference. Spectra were acquired with a 150 µm step size and raster width. Acquisition and subsequent processing were performed using the instrument software FlexImaging 4.1, ftmsControl, Flexcontrol and DataAnalysis form Bruker Daltonics (Bruker Daltonics, Bremen, Germany).

1.5 GC-MS and GC-C-IRMS Measurements

Averaged MSI enrichments were validated and complemented using gas chromatography mass spectrometry, which allow reliable and sensitive measurement. Enrichments of Phe and Tyr in tissue free amino acids (GC-MS) and protein-bound amino acids (GC-C-IRMS) were measured according to the protocols of Groen et al.[5] and Koopman et al.[6]

1.6 Histological Staining

MALDI is a non-destructive technique, which allows histological staining to be performed on the same tissue section after the imaging experiment. Hereto, the MALDI matrix was removed by washing in EtOH, and the tissue sections were stained with hematoxylin and eosin (H&E), which differentiates the nuclei from the cytoplasm of the cells in blue and red, respectively. Next, digital images of the stained tissues were made using a Mirax slide scanner (Zeiss, OberKochen, Germany) and co-registered with the MSI data (FlexImaging 4.1, Bruker Daltonics) to align the molecular distribution with the morphology of the liver tissue.

1.7 Data Analysis

MSI Data Preprocessing

After data acquisition, the obtained spectra were pre-processed to reduce the influence of instrumental and analytical variation. A total ion current filter was applied to distinguish off-tissue from on-tissue pixels. Subsequently, acquired spectra of all samples were normalized together by root mean square (RMS). The MATLAB scripts are available upon request.

Computation of Enrichment

A MATLAB script was developed to visualize the spatial localization of the tracer in tissues. MALDI-FTICR-MSI with high mass accuracy allowed to select target peaks based on the theoretical mass of the target analytes and the absolute isotopic mass difference between the tracer and tracee. An ion current filter was applied per pixel to avoid computing enrichments based on low intensity peaks originating from electronic and chemical noise. The tracer-to-tracee ratio (TTR) was calculated as the signal intensity of the stable isotope tracer (I_{tracer}) in relation to the intensity of the unlabeled analogue (I_{tracee}) at each pixel.

$$TTR = \frac{I_{tracer}}{I_{tracee}} \quad \text{(S1)}$$

If Equations (S2), (S3), and (S4) were satisfied:

- The *m/z* value of the observed peak was within 2 ppm of the theoretical *m/z*.

$$\frac{M_{obs} - M_{theo}}{M_{theo}} \cdot 1e^{-6} \leq 2\ ppm \quad \text{(S2)}$$

  where M_{obs} is the observed mass and M_{theo} the theoretical mass of the target peak.

- The absolute difference between the theoretical isotopic mass difference and the observed difference was below $1e^{-3}$ Da.

$$\Delta M_{obs} - \Delta M_{theo} \leq 1e^{-3} Da \quad \text{(S3)}$$

  Where

$$\Delta M_{obs} = M_{obs_{tracer}} - M_{obs_{tracee}}$$

$$\Delta M_{theo} = M_{theo_{tracer}} - M_{theo_{tracee}}$$

- The intensity of the analytes (tracer, tracee) was greater than the detection threshold:

$$I > 1e6 \quad \text{(S4)}$$

Molar percentage excess (MPE) was calculated using Equation (S5):

$$MPE = \frac{TTR}{TTR+1} \cdot 100 \quad \text{(S5)}$$

When the tracer was not detected, but the tracee was, TTR and MPE were set to 0. When both tracer and tracee were not detected (Equation (S4)), TTR and MPE were set to Not-a-Number (NaN).

The ratio of the irreversible conversion of Phe to Tyr by hydroxylation (Hydrox) was computed as:

$$Hydrox = \frac{MPE_{Tyr}}{MPE_{Phe}} \quad \text{(S6)}$$

Multivariate Analysis

Peak picking was performed using the mean spectrum with a signal to noise ratio (S/N) of 200.[7] The peak picked spectra were exported to MATLAB with a binning size of *m/z* of 0.001 Da to reduce data dimensionality for further analysis. Multivariate analyses were performed using the in-house ChemomeTricks toolbox for MATLAB.[7-8] Principal component analysis (PCA) is a linear unsupervised statistical method describing the largest variances within the dataset. Linear discriminant analysis (LDA) is a supervised method, which is used to associate features (*m/z* values) to specific classes. The analysis was performed according to the following pipeline:

1. The greatest variance in the dataset was observed from non-tissue-specific vs. tissue-specific signals. To reduce influences other than biological variance for further analysis, the first principal component was used to discard any non-tissue-specific signals, such as matrix and derivatization reagent peaks. Remaining peaks resulting from interactions between matrix and derivatization reagent were removed using the clustering method described by Billecke et al.[9]
2. PCA-LDA analysis was performed on 8 liver sections to associate time points with metabolic alterations.
3. PCA was performed on individual tissues to find the main sources of biological variance.

Integration of MSI Data with Public Databases

ID assignment of *m/z* values was done using the human metabolome database (www.hmdb.ca)[10] with a 2-ppm mass tolerance. Underivatized molecules were identified with a positive ion mass charge $[M + H]^+$; derivatized molecules $[M + TAHS]^+$ were obtained by subtraction of the monoisotopic mass value from the TAHS adduct in neutral ion mode [*M*] = [*m/z* – 177.1022394].

2. Schematic Overview of Mass Spectrometry Imaging (MSI) Workflow

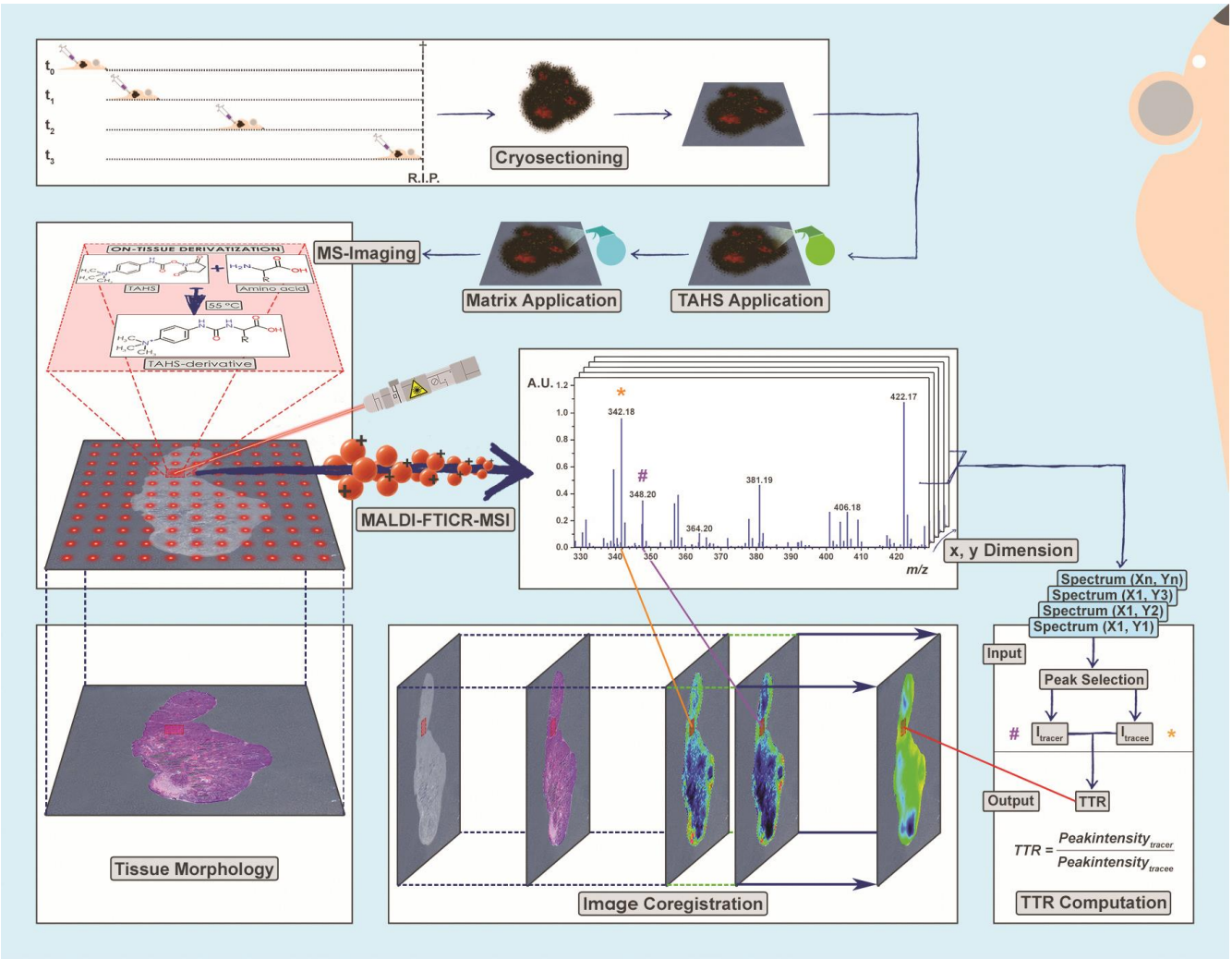

Figure S2. MALDI-MSI workflow to simultaneously visualize the *in situ* spatiotemporal distribution of Phe and other amino metabolites by using TAHS for on-tissue derivatization of fresh-frozen tumor and liver tissue derived from a H460 human NSCLC xenograft model. From the top left, mice were sacrificed at different time points after tracer injection and liver tissue was harvested, sectioned, and placed on ITO-coated slides. Next, tissues were derivatized with TAHS and coated with matrix before MALDI analysis. Enrichments were computed by processing the MSI data with a MATLAB algorithm (bottom right). Following MALDI, tissue sections were histologically stained (bottom left), digital images of which were coregistered with MSI images (bottom middle).

3. Preservation Spatial Analyte Localization

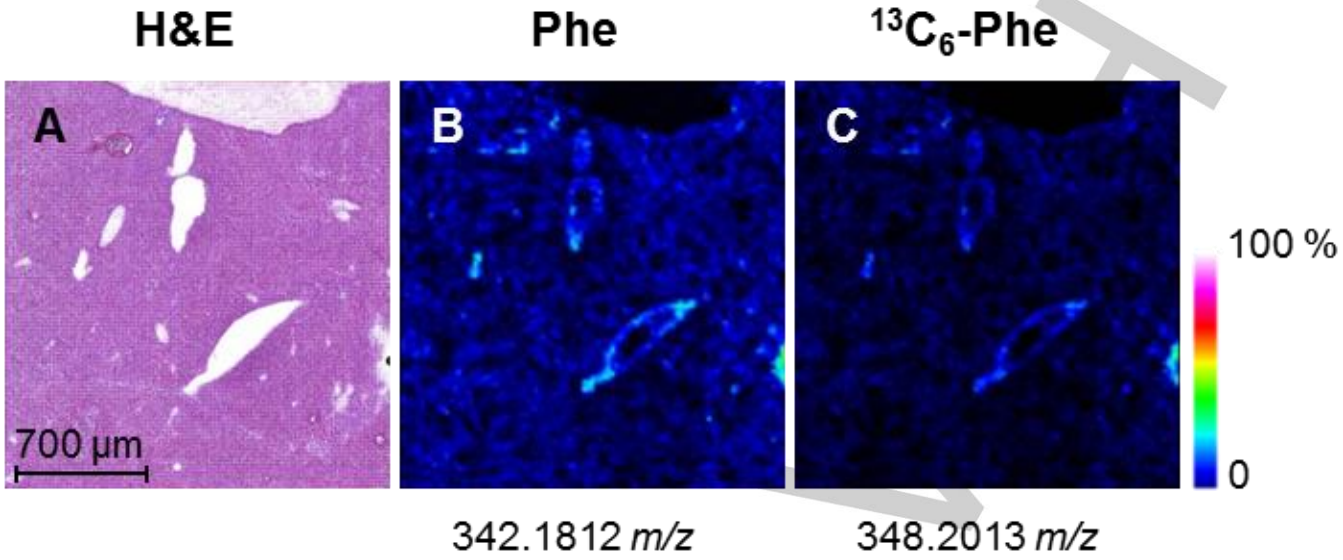

Figure S3. Preservation of the localization of Phe and $^{13}C_6$-Phe after on-tissue derivatization and matrix application. Both Phe (B) and $^{13}C_6$-Phe ($[M + TAHS]^+$) (C) were detected at a spatial resolution of 25 µm, and expressed as percentage of the maximal detected signal. Limited delocalization was observed as shown by the comparison of the clearly defined vascular structures in both the H&E (A) and MS-images (B-C).

4. Detection of Phe Derivatives by MS/MS Fragmentation

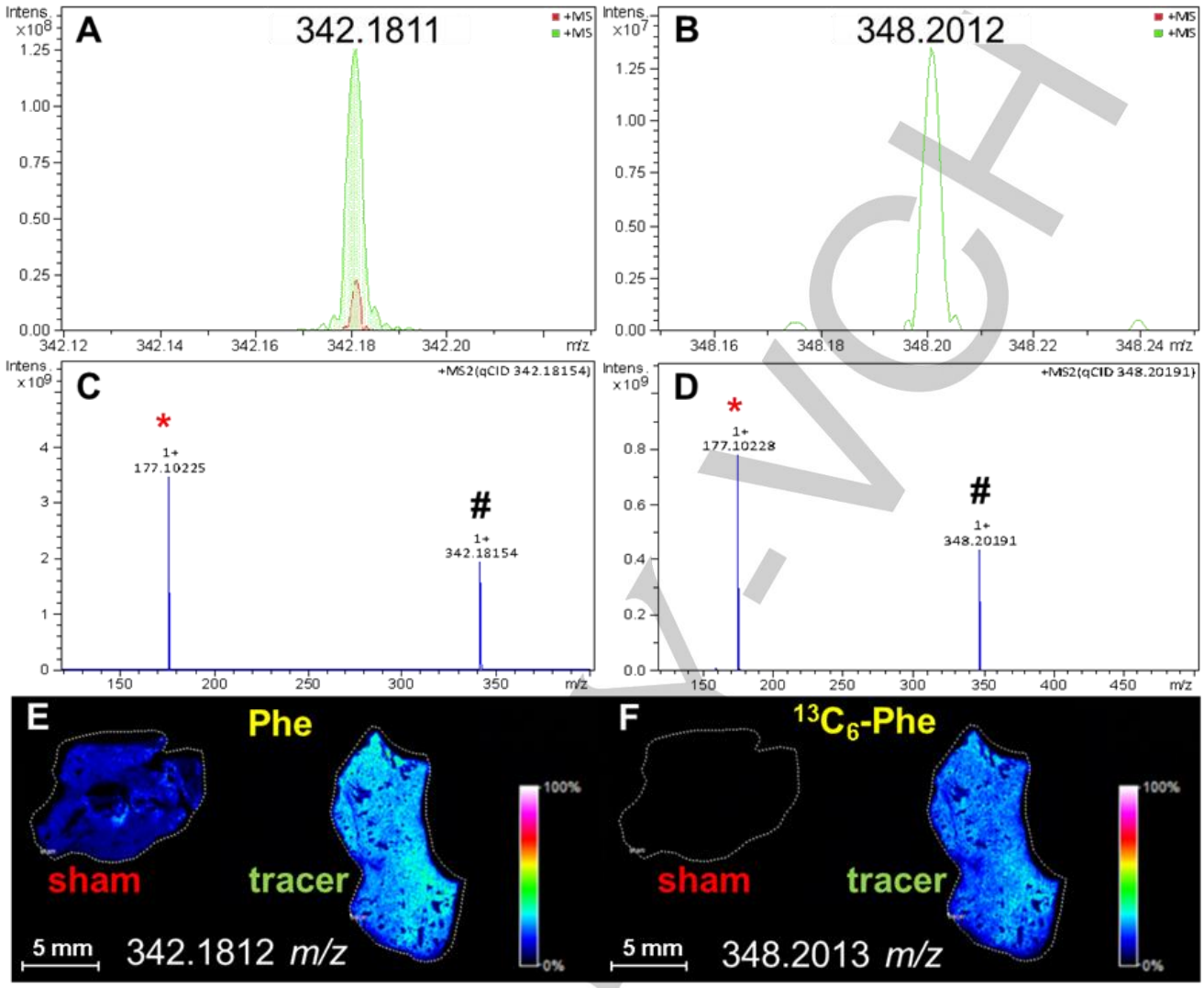

Figure S4. Specificity of the tracer detection in derivatized liver tissue. Both Phe (A,C,E) and 13C6-Phe (B,D,F) were detected in the liver of tracer-infused mice (green). Only Phe is detected in the sham-injected liver (red). Spectra show that, using high mass accuracy MS/MS (Bruker SolariX XR), the TAHS-specific fragment at 177.1022 *m/z* (*), is detected for both Phe and 13C6-Phe parent ions (#).

5. Identification of Derivatized Amino Compounds by MALDI-FTICR-MSI

Table S1. Amino acids identified in liver tissue by high-resolution MALDI-FTICR-MSI. The monoisotopic mass values ($Mass_{theo}$) are the sum of the neutral mass of the amino acid and the monoisotopic mass of the TAHS adduct ($C_{10}H_{13}N_2O$ $[M]^+$ = 177.1022394 *m/z*).

Compound	Chemical Formula[a]	Monoisotopic Mass $[M + TAHS]^+$	
		$Mass_{theo}$ (*m/z*)	Mass error (ppm)
Gly	$C_2H_5NO_2$	252.1343	-0.40
Ala	$C_3H_7NO_2$	266.1499	1.13
Ser	$C_3H_7NO_3$	282.1449	1.06
Pro	$C_5H_9NO_2$	292.1656	-1.37
Val	$C_5H_{11}NO_2$	294.1812	0.00
Thr	$C_4H_9NO_3$	296.1605	-1.01
Cys	$C_3H_7NO_2S$	298.1221	0.34
Tau	$C_2H_7NO_3S$	302.1169	0.99
Ile/ Leu	$C_6H_{13}NO_2$	308.1968	1.30
Asn	$C_4H_8N_2O_3$	309.1558	1.29
Orn	$C_5H_{12}N_2O_2$	309.1921	0.27
Asp	$C_4H_7NO_4$	310.1397	1.61
Gln	$C_5H_{10}N_2O_3$	323.1714	-0.62
Lys	$C_6H_{14}N_2O_2$	323.2077	1.55
Glu	$C_5H_9NO_4$	324.1554	-0.62
Met	$C_5H_{11}NO_2S$	326.1533	-0.31
His	$C_6H_9N_3O_2$	332.1718	-1.81
Phe	$C_9H_{11}NO_2$	342.1812	-0.05
ring-$^{13}C_6$-Phe	$C_9H_{11}NO_2$ [a]	348.2013	-0.42
Cit	$C_6H_{13}N_3O_3$	352.1979	0.77
Tyr	$C_9H_{11}NO_3$	358.1761	0.19
ring-$^{13}C_6$-Tyr	$C_9H_{11}NO_3$ [a]	364.1963	-0.17
Trp	$C_{11}H_{12}N_2O_2$	381.1921	0.26

[a]. ring-$^{13}C_6$-labeled analogues.

Table S2. Amino metabolites identified in liver tissue by high-resolution MALDI-FTICR-MSI. The monoisotopic mass values ($Mass_{theo}$) are the sum of the neutral mass of the amino acid and the monoisotopic mass of the TAHS adduct ($C_{10}H_{13}N_2O$ $[M]^+$ = 177.1022394 *m/z*).

		Monoisotopic Mass $[M + TAHS]^+$	
Compound	Chemical Formula	$Mass_{theo}$ (*m/z*)	Mass error (ppm)
Ammonia	NH_3	194.1288	2.12
Dimethylamine	C_2H_7N	222.1601	0.45
Urea	CH_4N_2O	237.1346	-1.70
Ethanolamine	C_2H_7NO	238.1550	0.74
Putrescine	$C_4H_{12}N_2$	265.2023	-0.74
Gamma-Aminobutyric acid	$C_4H_9NO_2$	280.1656	-1.31
Histamine	$C_5H_9N_3$	288.1819	1.09
Phenylethylamine	$C_8H_{11}N$	298.1914	-0.63
5-Oxoproline	$C_5H_7NO_3$	306.1448	1.20
Pipecolic acid	$C_6H_{11}NO_2$	306.1812	-0.06
Hydroxyproline	$C_5H_9NO_3$	308.1605	-0.92
Homocysteine	$C_4H_9NO_2S$	312.1376	-1.41
O-Phosphoethanolamine	$C_2H_8NO_4P$	318.1213	-0.44
Spermidine	$C_7H_{19}N_3$	322.2601	0.20
Xanthine	$C_5H_4N_4O_2$	329.1357	-1.41
Alanyl-Alanine	$C_6H_{12}N_2O_3$	337.1870	0.50
Putreanine/ Isoputreanine	$C_7H_{16}N_2O_2$	337.2234	-0.64
Aminoadipic acid	$C_6H_{11}NO_4$	338.1710	0.45
Serinyl-Glycine	$C_5H_{10}N_2O_4$	339.1663	-0.28
Uric acid	$C_5H_4N_4O_3$	345.1306	-1.10
1-Methyl-His/ 3-Methyl-His	$C_7H_{11}N_3O_2$	346.1874	-0.48
Gamma-N-Ethylglutamine	$C_7H_{14}N_2O_3$	351.2027	1.48
5-Hydroxytryptophane	$C_{10}H_{12}N_2O$	353.1972	0.00
Cysteinyl-Glycine	$C_5H_{10}N_2O_3S$	355.1435	-0.72
5-Hydroxykynurenamine	$C_9H_{12}N_2O_2$	357.1921	0.23
p-Serine	$C_3H_8NO_6P$	362.1112	0.09
Spermine	$C_{10}H_{26}N_4$	379.3180	0.57
Kynurenine	$C_{10}H_{12}N_2O_3$	385.1870	0.69
sn-Glycerophosphoethanolamine	$C_5H_{14}NO_6P$	392.1581	0.21
Alanyl-Glutamine	$C_8H_{15}N_3O_4$	394.2085	-0.75
Tetrahydrobiopterin	$C_9H_{15}N_5O_3$	418.2197	-1.26
Uridine	$C_9H_{12}N_2O_6$	421.1718	-1.37
Asparaginyl-Hydroxyproline	$C_9H_{15}N_3O_5$	422.2034	-0.50
gamma-Glutamyl-Cysteine	$C_8H_{14}N_2O_5S$	427.1646	-0.90
Inosine	$C_{10}H_{12}N_4O_5$	445.1830	0.43
Ophthalmic acid	$C_{11}H_{19}N_3O_6$	466.2296	1.23
Glutathione	$C_{10}H_{17}N_3O_6S$	484.1860	0.31
s-Adenosyl Homocysteine	$C_{14}H_{20}N_6O_5S$	561.2238	-1.12
LysoPE(18:0/0:0)	$C_{23}H_{48}NO_7P$	658.4191	0.18
Taurocholic acid	$C_{26}H_{45}NO_7S$	692.3939	-1.01
LysoPE(22:6(4Z,7Z,10Z,13Z,16Z,19Z)/0:0)	$C_{27}H_{44}NO_7P$	702.3878	-0.82
Oxidized Glutathione	$C_{20}H_{32}N_6O_{12}S_2$	789.2542	0.00

6. Recovery of $^{13}C_6$-Phe Enrichment on tissue by MALDI-FTICR-MSI

Two liver sections were spotted with 1 µL of 0.5 mM of Phe, which is much higher than Phe levels in tissue at 10 min. Although the Phe (Figure S4A) and $^{13}C_6$-Phe (Figure S4B) levels show a considerable amount of variation due to matrix effects (despite RMS normalization), MPE values (Figure S4C) show less variation and a high accuracy.

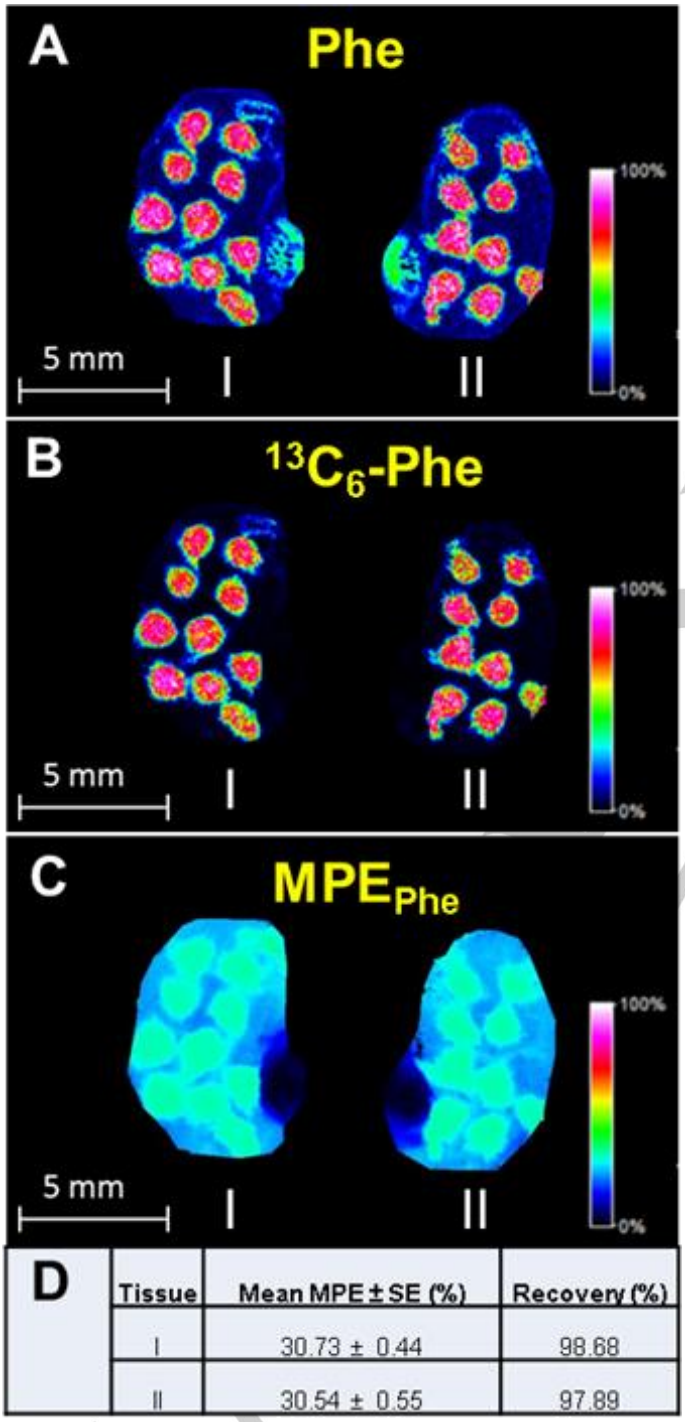

D

Tissue	Mean MPE ± SE (%)	Recovery (%)
I	30.73 ± 0.44	98.68
II	30.54 ± 0.55	97.89

Figure S5. Two consecutive liver sections (10 min) spotted with 1 µl of a 500µM solution containing $^{13}C_6$-Phe and Phe (4.4:5 (v:v)). Molecular ion [*M* + TAHS]$^+$ images of derivatized Phe (A) and derivatized $^{13}C_6$-Phe (B); C) MPE of $^{13}C_6$-Phe; D) Recovery computed by the average MPE values of the spotted pixels (% ± SE) of the number of spots (*n* = 9) per tissue.

7. Overall MPE of Tissue Free $^{13}C_6$-Phe and $^{13}C_6$-Tyr in Liver Tissue by MSI in comparison to GC-MS, and $^{13}C_6$-Phe Protein Enrichment by GC-C-IRMS

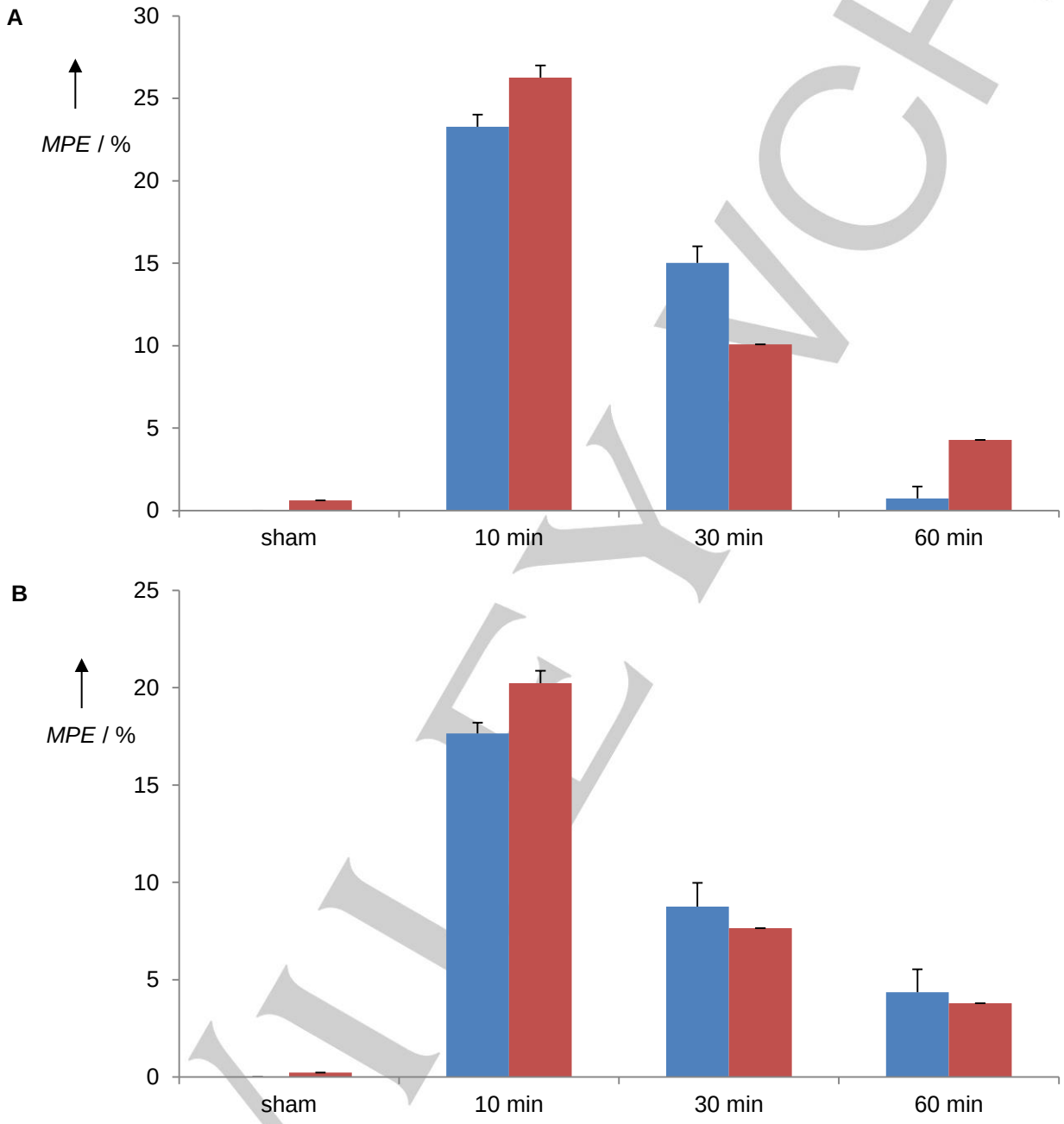

Figure S6. Enrichment of tissue-free $^{13}C_6$-Phe (A) and tissue-free $^{13}C_6$-Tyr (B) measured by MALDI-FTICR-MSI (blue) and GC-MS (red). Enrichment is shown as mean MPE ± SE (%), of all pixels for MSI, at the time points indicated. Each mean tissue value represents four biological replicates, each represented by the mean of two technical replicates.

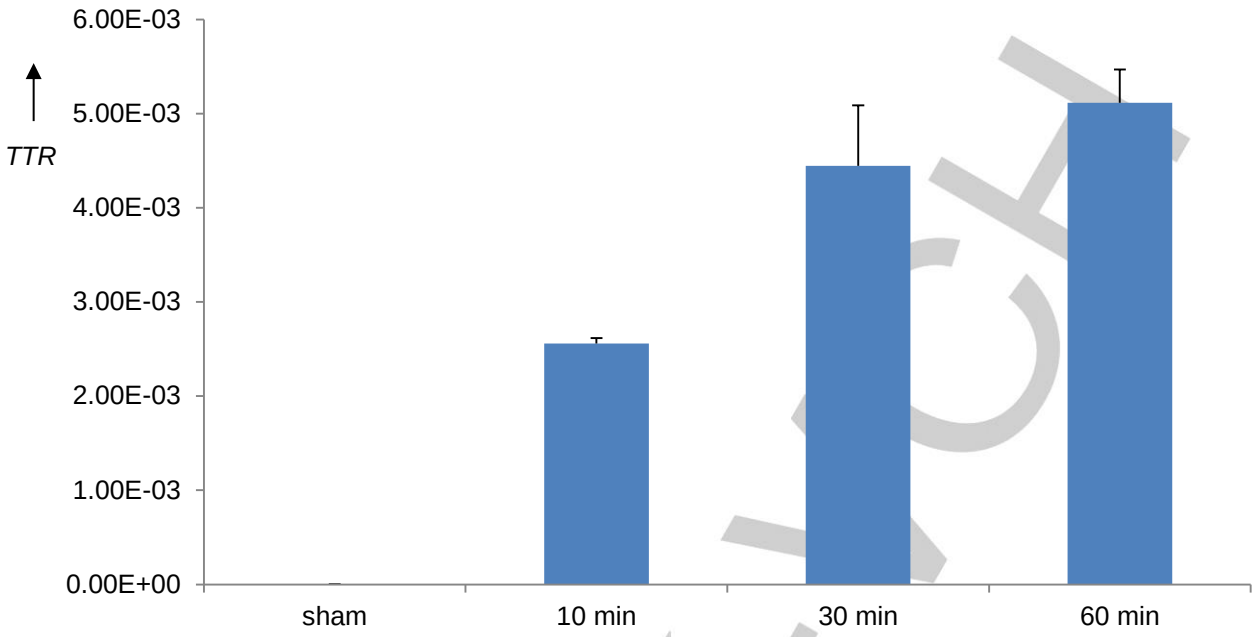

Figure S7. GC-C-IRMS measurement of $^{13}C_6$-Phe incorporation into hepatic proteins using tissue homogenates expressed as the TTR ± SE. Each mean tissue value represents four biological replicates, each represented by the mean of two technical replicates.

8. Tissue Specific Enrichments

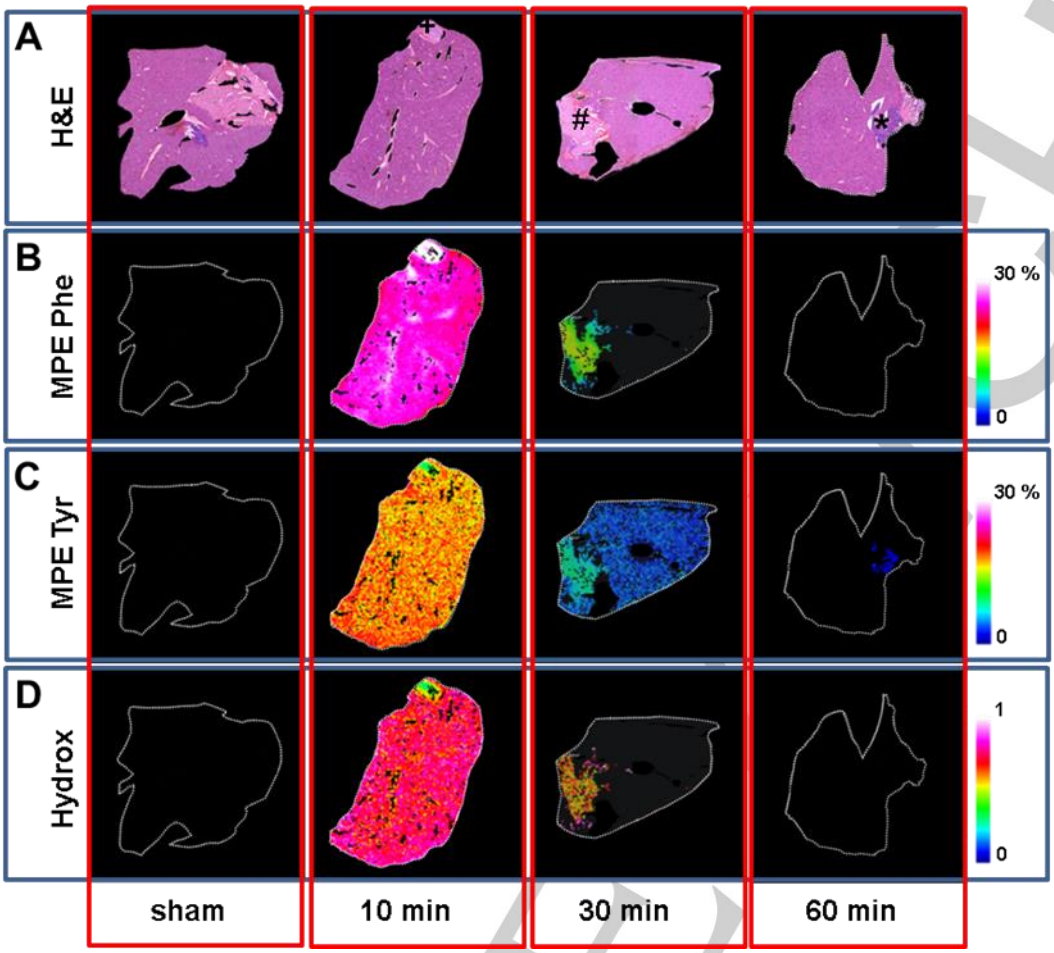

Figure S8. Visualization of 150 µm spatial Phe and Tyr kinetics in liver and adjacent tissues at three time points compared to control tissue (sham). A) H&E stains of liver tissue section with duodenum (+), muscle (#) and pancreas (*) tissue; B–D) Dynamic MS images for $^{13}C_6$-Phe MPE, $^{13}C_6$-Tyr MPE, and hepatic hydroxylation (Hydrox), respectively. Hydrox is expressed as the ratio of $^{13}C_6$-Tyr MPE: $^{13}C_6$-Phe MPE. Sections taken from mice 10 min after injection with saline (sham) are shown as a control.

9. Accuracy of Natural Phe and Tyr Enrichment by MALDI-FTICR-MSI

Table S3. Reconstructed natural enrichments compared to the theoretical ones. Isotopic ratios are defined as the intensity of the detected peak (M+1, M+2, M+3) divided by the intensity of the M+0 peak times 100%. The observed isotopic ratios are computed per pixel and presented here as the mean value ± SE for a tissue section at 10 min. The last column indicates the percentage of pixels in which a signal was detected.

Phe	Monoisotopic Mass (*m/z*)	Mass error (ppm)	Isotopic Ratio$_{theo}$ (%)[a]	Isotopic Ratio$_{obs}$ (%)	pixels ≥ 0 (%)
M+0	342.18120	-0.07	100.000	100.000	100.00
M+1	343.18460	0.15	20.549	19.741 ± 0.017	99.62
M+2	344.18794	0.75	2.000	1.479 ± 0.003	95.79
M+3	345.19130	1.36	0.123	0.106 ± 0.004	25.81

Tyr	Monoisotopic Mass (*m/z*)	Mass error (ppm)	Isotopic Ratio$_{theo}$ (%)	Isotopic Ratio$_{obs}$ (%)	pixels ≥ 0 (%)
M+0	358.17610	-0.12	100.000	100.000	100.00
M+1	359.17951	-0.09	20.549	18.072 ± 0.018	98.99
M+2	360.18286	0.81	2.000	1.231 ± 0.005	70.27
M+3	361.18622	0.87	0.123	1.327 ± 0.029	2.30

$^{13}C_6$-Phe	Monoisotopic Mass (*m/z*)	Mass error (ppm)	Isotopic Ratio$_{theo}$ (%)	Isotopic Ratio$_{obs}$ (%)	pixels ≥ 0 (%)
M+0	348.20130	-0.22	100.000	100.000	100.00
M+1	349.20469	0.14	14.064	12.062 ± 0.017	95.90
M+2	350.20804	1.54	0.912	0.576 ± 0.010	29.64
M+3	351.21140	-0.03	0.036	1.155 ± 0.039	0.43

$^{13}C_6$-Tyr	Monoisotopic Mass (*m/z*)	Mass error (ppm)	Isotopic Ratio$_{theo}$ (%)	Isotopic Ratio$_{obs}$ (%)	pixels ≥ 0 (%)
M+0	364.19630	0.41	100.000	100.000	100.00
M+1	365.19961	0.75	14.064	11.298 ± 0.028	83.85
M+2	366.20296	0.10	0.912	4.536 ± 0.097	1.72
M+3	367.20632	-0.28	0.036	9.780 ± 0.189	0.22

[a]. The theoretical isotope pattern for ^{13}C was calculated using the Isotope Distribution Calculator and Mass Spec Plotter from the MS online tools from sisweb.com (Scientific Instrument Services, Ringoes, NJ, USA). The chemical formula of the derivatized amino acid $[M+TAHS]^+$ was used, and the high resolution calculation method was selected.

10. Principal Component Analysis and Linear Discriminant Analysis

10.1 PCA-LDA Analysis at Different Time Points

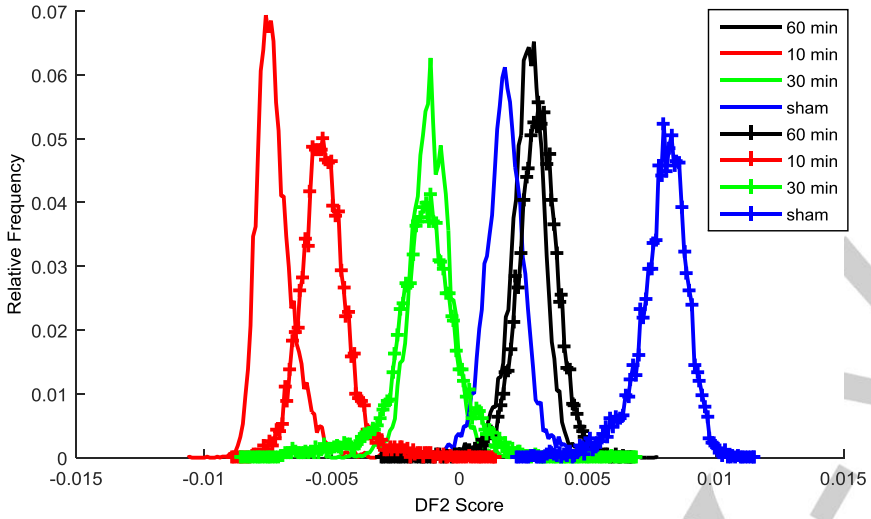

Figure S9. Second discriminant function based on 8 liver tissues (2 sections each at 3 time points as well as 2 control (sham) sections). Discriminant analysis enabled the distinction between samples exposed to tracer and samples that were either never exposed to the tracer bolus or from which tracer was cleared from the tissue (negative and positive function, respectively).

Table S4. Overview of amino acids in the positive and negative component of discriminant function 2.

Negative discriminant function			Positive discriminant function		
Mass (*m/z*)	Loading	Compound	Mass (*m/z*)	Loading	Compound
348.2012	-0.72	$^{13}C_6$-Phe	292.1652	0.52	Pro
342.1812	-0.34	Phe	308.1962	0.48	Leu/ Ile
379.3172	-0.21	Spermine	294.1812	0.41	Val
238.1552	-0.21	Ethanolamine	252.1342	0.41	Gly
318.1212	-0.11	O-Phosphoethanolamine	323.2072	0.38	Lys
358.1762	-0.07	Tyr	381.1912	0.37	Trp
322.2602	-0.06	Spermidine	309.1922	0.31	Orn
306.1442	-0.05	5-Oxoproline	392.1572	0.31	sn-Glycerophosphoethanolamine
324.1622	-0.03	Gly	332.1712	0.30	His
			323.1712	0.30	Gln
			484.1862	0.25	Glutathione
			309.1552	0.24	Asn
			338.1712	0.21	Aminoadipic acid
			298.1222	0.17	Cys
			296.1602	0.04	Thr
			789.2542	0.04	Oxidized Glutathione

10.2 PCA Analysis and Morphological Differences in a Single Tissue

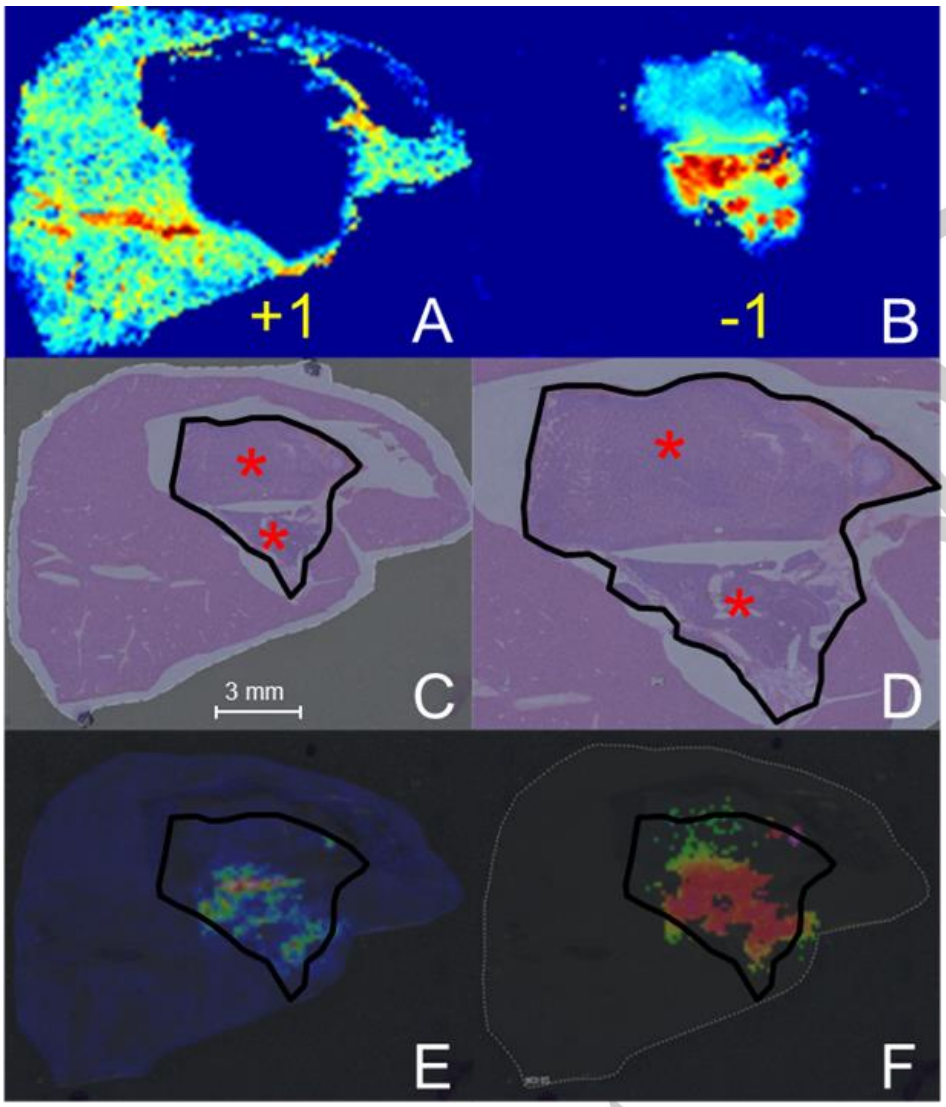

Figure S10. PCA analysis of MSI data versus morphology assessed by an H&E stain in liver tissue taken 30 min post-injection. A, B) Visualization of the first principal component (PC1): The positive PC1 (A) mainly comprises liver tissue, and the negative PC1 (B), pancreas tissue (B). C) H&E stain of liver section, containing liver and pancreas tissue (*); D) Zoom (2× magnification) of the H&E stain shown in C. E, F) MS- images of $^{13}C_6$-Phe (E, $[M + TAHS]^+$ (*m/z*)) and $^{13}C_6$-Phe MPE (F, %).

Table S5. Overview of the amino acids and amine-metabolites observed in the positive and negative function of the first principal component (PC1). The positive function (PC+1) mainly comprises liver tissue, and the negative PC1, pancreas tissue (PC-1).

	PC +1			PC -1	
Mass (*m/z*)	Loading	Compound	Mass (*m/z*)	Loading	Compound
323.1712	0.64	Glu	318.1212	-0.91	O-p-ethanolamine
332.1712	0.57	His	348.2012	-0.55	$^{13}C_6$-Phe
484.1862	0.45	Glutathione	358.1762	-0.53	Tyr
302.1172	0.34	Tau	342.1812	-0.52	Phe
323.2072	0.12	Lys	322.2602	-0.52	Spermidine
			252.1342	-0.49	Gly
			338.1712	-0.46	Aminoadipic acid
			238.1552	-0.43	Ethanolamine
			381.1922	-0.42	Trp
			296.1602	-0.41	Thr
			292.1652	-0.26	Pro
			294.1812	-0.13	Val
			266.1502	-0.09	Ala

11. NMR Spectra

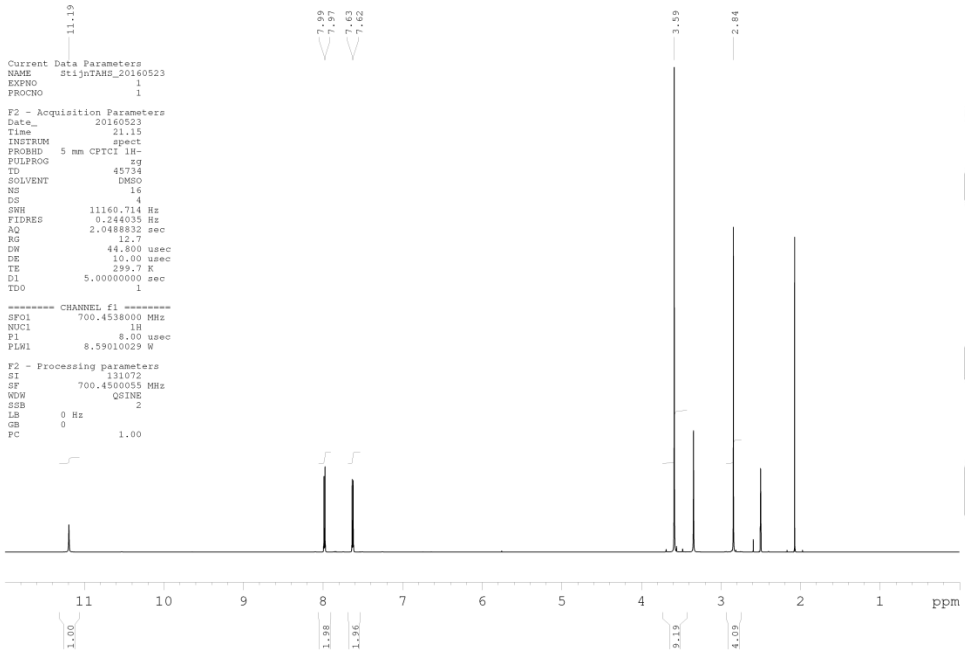

Figure S11. ^{1}H spectrum of synthesized TAHS.

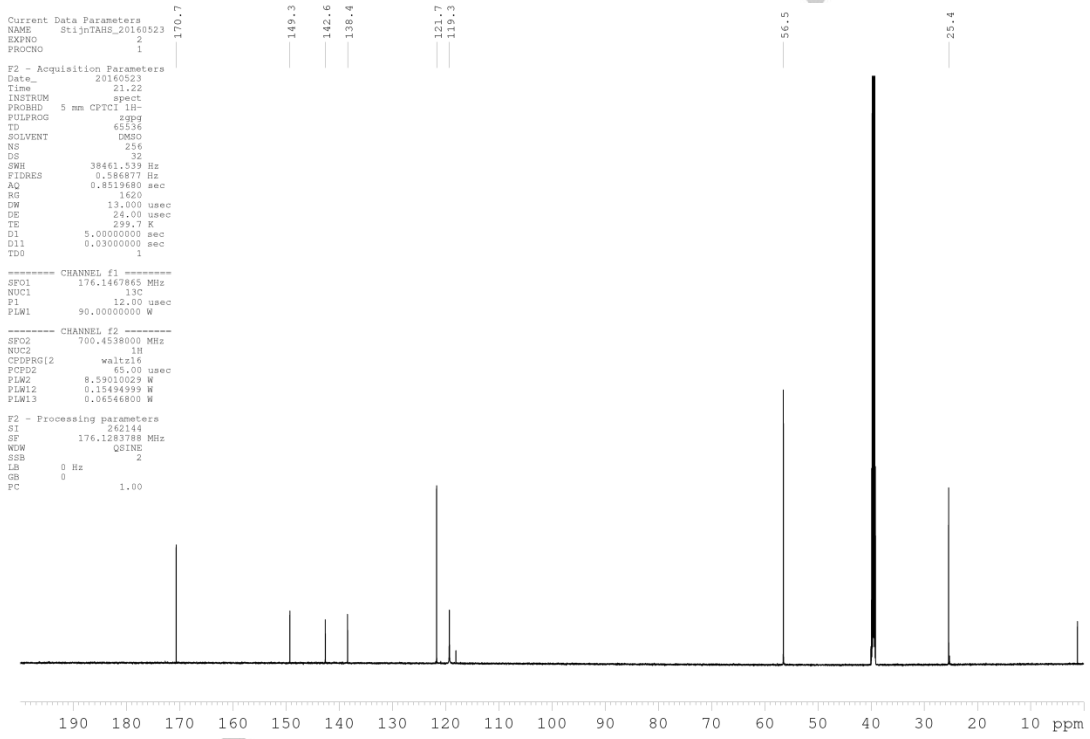

Figure S12. ^{13}C spectrum of synthesized TAHS.

References

[1] K. Shimbo, A. Yahashi, K. Hirayama, M. Nakazawa, H. Miyano, *Anal Chem* **2009**, *81*, 5172-5179.

[2] N. A. Burd, H. M. Hamer, B. Pennings, W. F. Pellikaan, J. M. Senden, A. P. Gijsen, L. J. van Loon, *PLoS One* **2013**, *8*, e68109.

[3] S. G. Peeters, C. M. Zegers, R. Biemans, N. G. Lieuwes, R. G. van Stiphout, A. Yaromina, J. D. Sun, C. P. Hart, A. D. Windhorst, W. van Elmpt, L. J. Dubois, P. Lambin, *Clin Cancer Res* **2015**, *21*, 2984-2992.

[4] C. Esteve, E. A. Tolner, R. Shyti, A. M. van den Maagdenberg, L. A. McDonnell, *Metabolomics* **2016**, *12*, 30.

[5] B. B. Groen, A. M. Horstman, H. M. Hamer, M. de Haan, J. van Kranenburg, J. Bierau, M. Poeze, W. K. Wodzig, B. B. Rasmussen, L. J. van Loon, *PLoS One* **2015**, *10*, e0141582.

[6] R. Koopman, N. Crombach, A. P. Gijsen, S. Walrand, J. Fauquant, A. K. Kies, S. Lemosquet, W. H. Saris, Y. Boirie, L. J. van Loon, *Am J Clin Nutr* **2009**, *90*, 106-115.

[7] G. B. Eijkel, B. Kükrer Kaletaş, I. M. van der Wiel, J. M. Kros, T. M. Luider, R. M. A. Heeren, *Surface and Interface Analysis* **2009**, *41*, 675-685.

[8] F. Gerber, F. Marty, G. B. Eijkel, K. Basler, E. Brunner, R. Furrer, R. M. Heeren, *Anal Chem* **2013**, *85*, 10249-10254.

[9] N. Billecke, G. Rago, M. Bosma, G. Eijkel, A. Gemmink, P. Leproux, G. Huss, P. Schrauwen, M. K. Hesselink, M. Bonn, S. H. Parekh, *Histochem Cell Biol* **2014**, *141*, 263-273.

[10] C. A. Smith, G. O'Maille, E. J. Want, C. Qin, S. A. Trauger, T. R. Brandon, D. E. Custodio, R. Abagyan, G. Siuzdak, *Ther Drug Monit* **2005**, *27*, 747-751.

Author Contributions

Martijn Arts:
Conceptualization: Equal
Data curation: Equal
Formal analysis: Lead
Methodology: Equal
Software: Supporting
Writing – original draft: Equal
Writing – review & editing: Equal
Animal experiments: Equal

Zita Soons:
Conceptualization: Equal
Data curation: Equal
Methodology: Equal
Supervision: Lead
Writing – original draft: Equal
Writing – review & editing: Lead

Shane R. Ellis:
Conceptualization: Supporting
Methodology: Supporting
Supervision: Supporting
Writing – original draft: Supporting
Writing – review & editing: Supporting

Keely A. Pierzchalski:
Supervision: Supporting
Writing – review & editing: Supporting

Benjamin Balluff:
Data curation: Supporting
Writing – review & editing: Supporting

Gert. B. Eijkel:
Data curation: Supporting
Software: Lead

Ludwig J. Dubois:
Funding acquisition: Supporting
Methodology: Supporting
Resources: Supporting
Supervision: Supporting
Writing – review & editing: Supporting

Natasja G. Lieuwes:
Methodology: Supporting
Animal experiments: Equal

Stijn M. Agten:
Writing – review & editing: Supporting
TAHS reagent production: Lead

Tilman M. Hackeng:
Data curation: Supporting
Resources: Supporting
Supervision: Supporting

Luc J.C. van Loon:
Data curation: Supporting
Methodology: Supporting
Resources: Supporting
Writing – review & editing: Supporting

Ron M.A. Heeren:
Conceptualization: Equal
Data curation: Supporting
Funding acquisition: Equal
Methodology: Supporting

Resources: Equal
Supervision: Supporting
Writing – review & editing: Supporting

Steven W.M. Olde Damink:
Conceptualization: Equal
Funding acquisition: Equal
Methodology: Supporting
Resources: Equal
Supervision: Supporting
Writing – review & editing: Supporting